ACS NANO
Cite This: ACS Nano 2019, 13, 1595−1602
www.acsnano.org

ARTICLE

Engineering Point-Defect States in Monolayer WSe_2

Chendong Zhang,*,†,‡,# Cong Wang,§,# Feng Yang,§ Jing-Kai Huang,∥ Lain-Jong Li,∥ Wang Yao,⊥ Wei Ji,*,§ and Chih-Kang Shih*,‡

†School of Physics and Technology, Wuhan University, Wuhan 430072, China
‡Department of Physics, University of Texas at Austin, Austin, Texas 78712, United States
§Department of Physics and Beijing Key Laboratory of Optoelectronic Functional Materials and Micro-Nano Devices, Renmin University of China, Beijing 100872, China
∥Physical Sciences and Engineering Division, King Abdullah University of Science and Technology, Thuwal 23955-6900, Kingdom of Saudi Arabia
⊥Department of Physics and Center of Theoretical and Computational Physics, University of Hong Kong, Hong Kong, China

Supporting Information

ABSTRACT: **Defect engineering is a key approach for tailoring the properties of the emerging two-dimensional semiconductors. Here, we report an atomic engineering of the W vacancy in monolayer WSe_2 by single potassium atom decoration. The K decoration alters the energy states and reshapes the wave function such that previously hidden midgap states become visible with well-resolved multiplets in scanning tunneling spectroscopy. Their energy levels are in good agreement with first-principle calculations. More interestingly, the calculations show that an unpaired electron donated by the K atom can lead to a local magnetic moment, exhibiting an on−off switching by the odd−even number of electron filling. Experimentally the Fermi level is pinned above all defect states due to the graphite substrate, corresponding to an off state. The close agreement between theory and experiment in the off state, on the other hand, suggests the possibility of gate-programmable magnetic moments at the defects.**

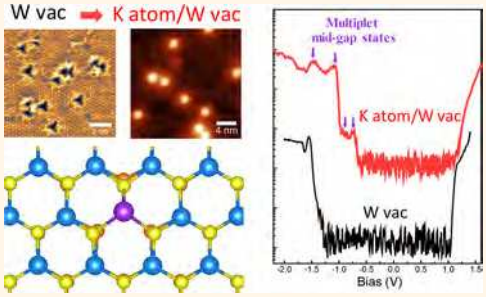

KEYWORDS: *transition metal dichalcogenides, defect engineering, midgap defect states, local magnetic moment, spin splitting*

Atomically thin transition-metal dichalcogenides (TMDs) have attracted great interest in both fundamental science and device applications.[1−6] Point defects in monolayer TMDs play significant roles in many aspects.[7−11] For example, the vacancies are believed to alter the work function, determine the type of majority carrier,[12,13] and notably affect carrier transport.[12,14] In photoluminescence, the localized point defect states can lead to the confinement of excitons, allowing for the realization of highly efficient single-photon sources.[15−17] To understand these intriguing properties, it is of fundamental importance to establish the correlations between the atomic configurations and the electronic structures of point defects. By means of transmission electron microscope, various atomic configurations for point defects in monolayer (ML) TMDs have been reported.[18−20] For most of them, midgap defect states were theoretically predicted,[21−23] but thus far, such predictions are only supported indirectly using electron transport and optical spectroscopy. Scanning tunneling microscope/spectroscopy (STM/S) is a powerful tool to unravel this issue. However, in previous STS studies of the point defect in ML TMD, such localized midgap defect states were not observed,[24−26] leaving this issue unresolved. On the other hand, defect engineering, which tunes the localized defect electronic structures, can be a powerful strategy to realize and to expand the technological potential of 2D semiconducting materials. So far, the experimental work that directly reveals how the modification of atomic configuration can alter localized defect electronic structures in monolayer TMDs has rarely been reported.

Here, we report an approach to engineering W vacancy (W_{vac}) in ML-WSe_2 by a single potassium atom decoration. Combining scanning tunneling microscopy/spectroscopy and first-principles calculations, both the atomic structure and the modulated electronic structures of the potassium atom decorated W vacancy (*i.e.*, K/W_{vac}) are unveiled. We show that the potassium atom adsorption reshapes the wave functions of these defect states, which therefore, leads to the localized midgap states extending further into vacuum. This reshaping of the wave function is primarily responsible for the

Received: October 5, 2018
Accepted: January 28, 2019
Published: January 28, 2019

DOI: 10.1021/acsnano.8b07595
ACS Nano 2019, 13, 1595−1602

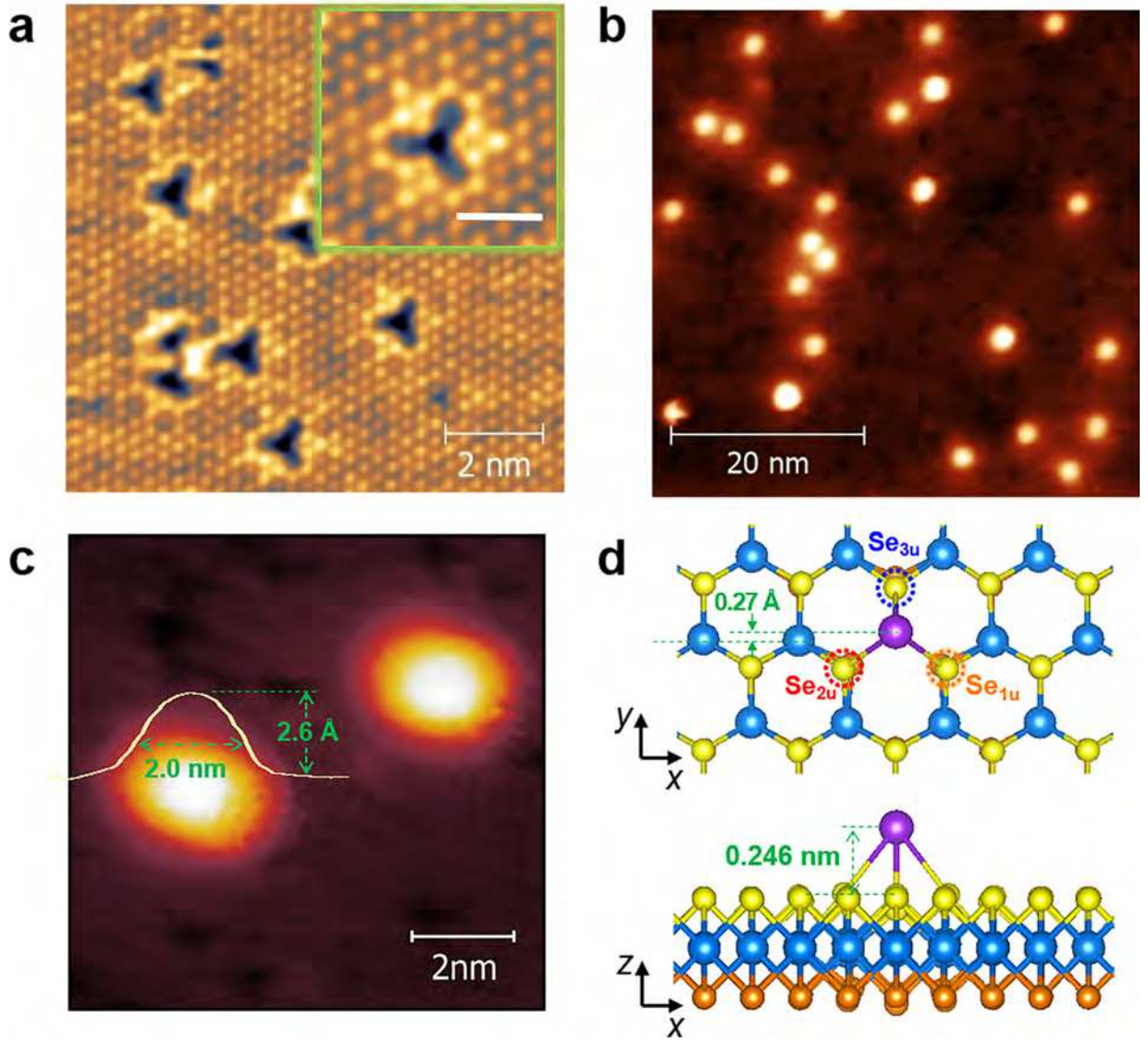

Figure 1. STM images and the atomic model of K/W_{vac}. (a) Atomically resolved STM image of intrinsic W vacancies in ML-WSe_2. A close-up image is shown in the inset. (b) STM image after the deposition of potassium and subsequent annealing. (c) Zoomed-in image of (b). Typical height profile of the K/W_{vac} complex is displayed with the lateral diameter and the height labeled. (d) Schematic model of the most stable configuration of a single K atom adsorbed on W_{vac}. The top view and side view are shown in the upper and lower panels, respectively. Three nearby Se atoms are labeled as shown. Scanning parameters: (a) −1.45 V, 10 pA; (b) and (c) −1.0 V, 8 pA. Scale bar is 1 nm in the inset of (a).

visibility of these defect states. The multiplet structures of such defect states are directly observed by using STS, and their energy levels are in good agreement with theoretical calculations. More interestingly, the calculations show that the donated charge from the K atom to surrounding Se and W atoms can lead to a local magnetic moment which lifts the spin degeneracy of the defect states (as large as 168 meV). The magnetic moment and spin splitting exhibit an on and off switching, by the odd and even electron filling of defect states. In our experiments, the graphite substrate pins the Fermi level of ML-WSe_2, above all defect states, corresponding to an off state of the magnetism. This finding points to the possibility of programming the magnetic moment at point defects by placing them on a substrate whose Fermi level can be tuned by gating.

RESULTS AND DISCUSSION

The monolayer WSe_2 was grown on highly oriented pyrolytic graphite (HOPG) by chemical vapor deposition following the same procedure used in ref 26. The atomically resolved STM image of the ML-WSe_2 shows a random distribution of point defects on the surface (Figure 1a). The inset in Figure 1a is a close-up image of a single vacancy, exhibiting a trefoil-like shape. According to previous studies,[27−31] chalcogen atoms at a TMD surface are imaged in STM measurements under usual tunneling conditions, showing a hexagonal lattice. Therefore, the majority of vacancies observed in our studies are centered on the tungsten sites. This observation, and the dI/dV spectrum of the vacancy (the orange curve in Figure 2a), are consistent with previous research.[26] We note that chalcogen vacancy has also been reported in ML TMDs recently, and the oxygen passivation was proposed as the reason for the missing of midgap states.[32,33] As discussed in the Supporting

DOI: 10.1021/acsnano.8b07595
ACS Nano 2019, 13, 1595−1602

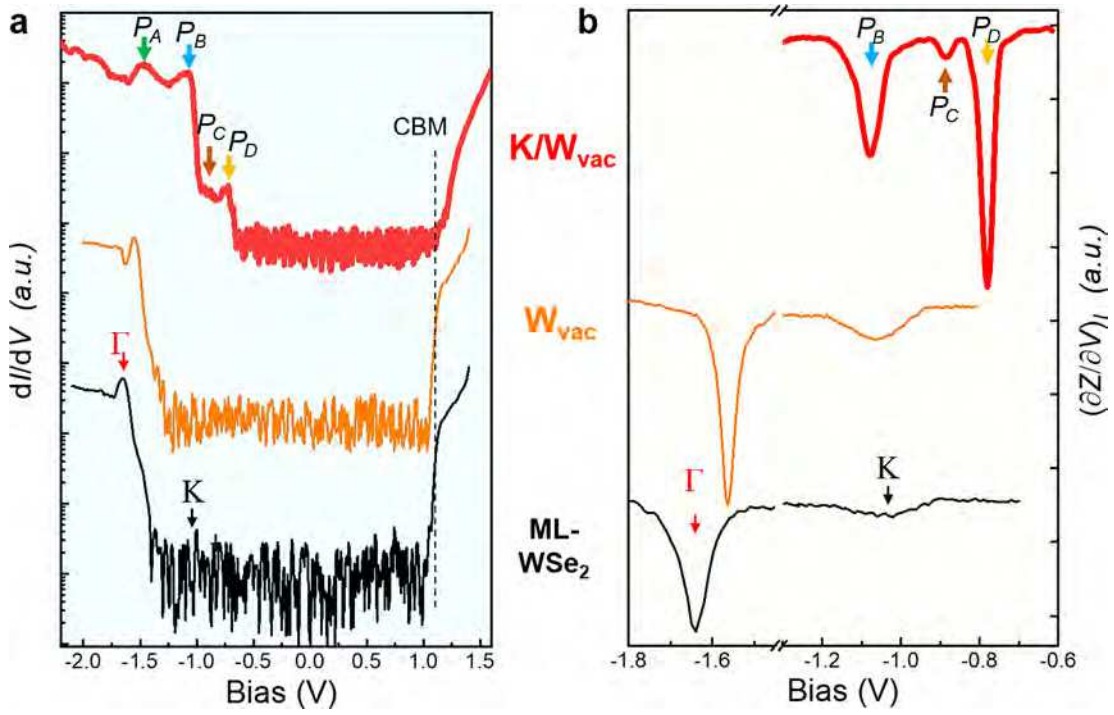

Figure 2. STS investigations of W_{vac}. (a) Logarithm of dI/dV spectra for K/W_{vac} (red), intrinsic W_{vac} (orange), and the ML-WSe_2 (black). The band edge states of ML-WSe_2 at the Γ and K points are indicated by red and black arrows, respectively. The conduction band minimums (CBM) are labeled for all three situations with black dashed line. (b) Corresponding $(\partial Z/\partial V)_I$ spectra for the valence bands. Four defect states are labeled as P_A, P_B, P_C, and P_D in the spectra of K/W_{vac}.

Information (Figures S1 and S2 and Table S1), the electronic structures of the K-decorated Se vacancy or oxidized Se vacancy are not consistent with our STS measurements of the K-decorated vacancy defect. Therefore, we believe that, in our work, W_{vac} is the dominant type of point defects. Since the defect types and densities severely depend on the sample growth conditions, the defect types reported here might be different from those of refs 32 and 33.

Potassium atoms were deposited on the WSe_2 surface at room temperature using a SAES Getters alkali metal dispenser in a standard molecular beam epitaxy chamber (see the Methods). As-deposited potassium atoms tend to form different-size small clusters on the surface (as displayed in Figure S3). After the sample was annealed at 450 K for 30 min, discrete and randomly distributed protrusions with uniform diameter were observed on the WSe_2 surface (Figure 1b). Such a bright spot can be removed by a STM tip with a relatively strong tip−sample interaction. A vacancy was always found after the on-top K atom was removed (Figure S4). This experimental observation agrees with the first-principles calculations, which indicates that the thermally favored adsorption site for a potassium atom is on top of a W_{vac} (Figure 1d). In our calculations, a 7 × 7 parallelogram supercell was adopted to model the adsorption of a single K atom on WSe_2 (see the Methods). We have carefully examined nine possible adsorption sites (see details in Figure S5 and Tables S2 and S3). Figure 1d illustrates the fully relaxed atomic structure of the most stable configuration for a K/W_{vac} complex. Three Se atoms in the upper Se layer surrounding the missing W atom are labeled as Se_{1u}, Se_{2u}, and Se_{3u}. As seen in the top-view image (the upper panel in Figure 1d), the K atom sits slightly off the center of the W vacancy (*i.e.*, the position of the missing W atom), displaced toward Se_{3u} along the *y* direction by 0.27 Å. Therefore, it leads to a substantial structural distortion of the surrounding Se atoms and unequal distances of the K atom to Se_{1u}−Se_{3u}. For instance, in the out-of-plane direction, Se_{3u} is lowered by 0.34 Å, while Se_{1u} and Se_{2u} move upward by 0.15 and 0.19 Å, respectively. The side view (lower panel of Figure 1d) shows that the K atom resides over the upper Se layer by 2.46 Å, consistent with the experimental height profile shown in the inset of Figure 1c. The apparent diameter of the protrusion measured in Figure 1c is 1.98 ± 0.15 nm (statistic distribution can be seen in Figure S6), comparable with the in-plane distribution of the defect states wave functions (see Figure S7).

The electronic structures of K/W_{vac} were examined using scanning tunneling spectroscopy. The red curve in Figure 2a represents a typical dI/dV spectrum taken on K/W_{vac}. For comparison, the spectra of a clean WSe_2 monolayer and an intrinsic W vacancy are displayed by the black and orange curves, respectively. Potassium surface doping has been widely used in photoemission studies of semiconductors to shift their Fermi levels into unoccupied states.[34−36] In our case, however, the adsorption of a single potassium atom on W_{vac} shows different spectroscopic features. The most pronounced feature in the tunneling spectra, as shown in Figure 2a,b, lies in the emerged occupied states (labeled as P_A, P_B, P_C, and P_D) within the apparent bandgap of ML-WSe_2. Multiple measurements have been taken on different K/W_{vac} sites over the sample surface. They all show consistent topographic and electronic structures (see Figure S8). Statistical analysis reveals that the energy levels of P_A, P_B, P_C, and P_D are −1.46 ± 0.06, −1.12 ± 0.07, −0.91 ± 0.07, and −0.80 ± 0.06 eV, respectively. We point out that in the dI/dV spectrum (Figure 2a), P_C only appears as a weak shoulder between the P_B and P_D peaks. This is because the regular dI/dV spectroscopy lacks the sensitivity

DOI: 10.1021/acsnano.8b07595
ACS Nano 2019, 13, 1595−1602

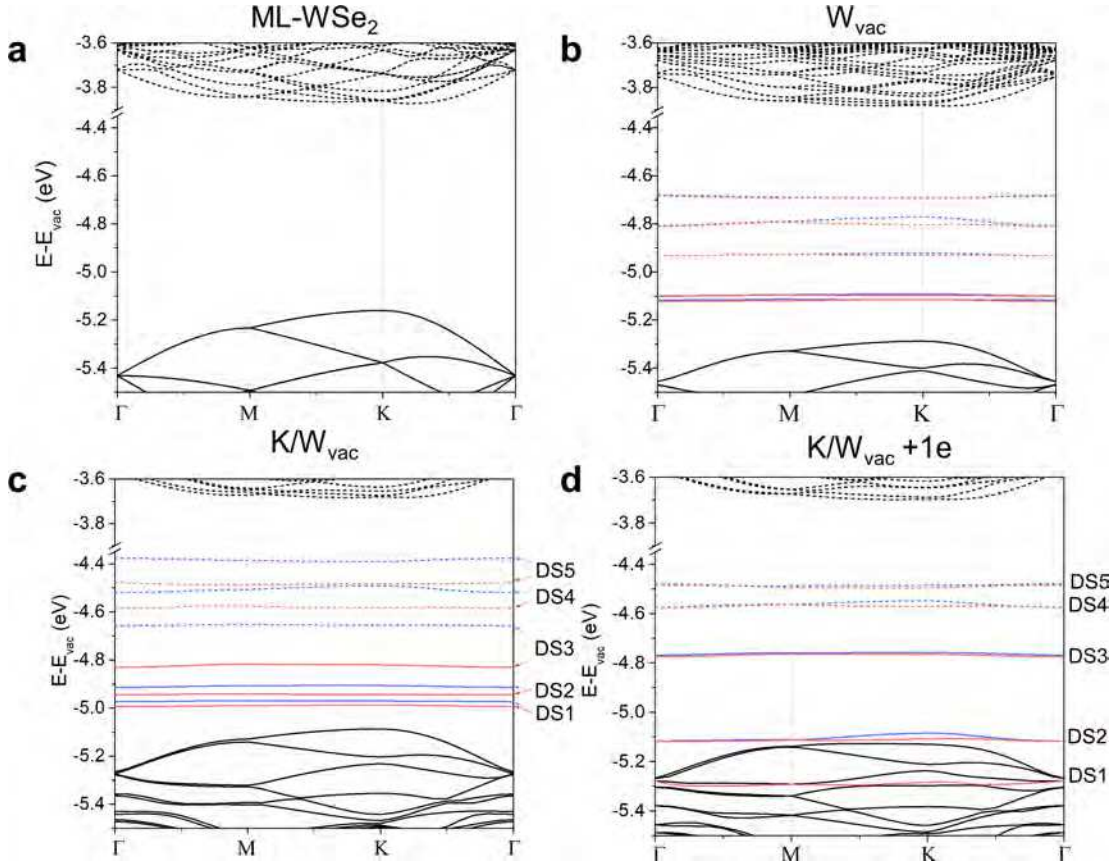

Figure 3. Theoretical band structures calculated with consideration of spin-orbit coupling (SOC). (a) ML-WSe_2 in a 7 × 7 supercell, (b) a tungsten vacancy (W_{vac}) in the supercell, (c) a single K atom decorated W_{vac} (K/W_{vac}), (d) one additional electron doped K/W_{vac}. The energy scale is relative to the vacuum level. In each panel, solid and dashed lines represent occupied and unoccupied bands, respectively. To highlight the mid-gap defects states, we used blue and red colors to distinguish the two spin-resolved states from the same origin. The red band always has a lower energy than the blue band. A pair of red and blue bands denote a defect state, e.g. DS1 to DS5, as labeled in (c) and (d).

to reveal the detailed band edge structures of ML TMD materials, as we reported earlier.[37] By taking advantage of the constant tunneling current spectroscopy in revealing individual energy thresholds, P_C can be clearly observed as a dip in the $(\partial Z/\partial V)_I$ spectrum shown in Figure 2b.

To understand these spectroscopic features, we examined our DFT results for the electronic structures of K/W_{vac}. Parts a−c of Figure 3 show the theoretical band structures of ML-WSe_2, W_{vac}, and K/W_{vac}, respectively, with their vacuum levels aligned. Five midgap defect states are introduced by the W vacancy, labeled as DS1-DS5 in Figure 3b, corresponding to the breakdown of six 4/3 electron filled W−Se bonds and the removal of the two remaining nonbonded *d* electrons of W. However, most of the midgap defect states of the intrinsic W_{vac} were not observed by STS measurements (see the orange curves in Figure 2 and ref 26). As discussed in Figure S7, we believe that this is likely due to the mostly in-plane spatial distributions of the wave functions of the defect states. The decoration of a potassium atom does not change the number of defect states but shifts their energy levels (Figure 3c) and pulls the spatial distribution of defect states wave functions toward the vacuum. Figure 4 shows the K decoration induced radial difference of the wave function norms of DS2-DS5 at the K point. One can see that compared with the intrinsic W_{vac}, the wave functions of the defect states now extend further in the *Z* direction, where the charge densities in the region being 1−2 Å above the K atom are notably enhanced. As a result, it enables the direct probe of the midgap point defect states by tunneling spectroscopy.

Most interestingly, as shown in Figure 3c, the spin degeneracies of the defect states are lifted by the potassium atom adsorption, indicating the defect has acquired a magnetic moment. The DS3 and DS5 states have relatively large splits (Δ_{SS}) of 168 and 75 meV, respectively. The Δ_{SS} of other defect states are also enlarged by several tens of meV, in comparison to the intrinsic W_{vac} (Table S4). A small dispersion appears for the defect levels in Figure 3c. This is simply due to the periodic boundary condition imposed in the supercell calculation, while in reality these levels should be flat throughout the Brillouin zone. The presented values of Δ_{SS} are averages over the Brillouin zone of the supercell used in the calculations. The calculations in Figure 3a−c are based on free-standing WSe_2 without a substrate, in which the Fermi level (E_F) reflects the charge neutrality condition. For W_{vac}, E_F is located above the spin degenerate DS1 and DS2 (Figure 3b). For the K/W_{vac} complex, one additional electron is filled into the DS3 level, which leads to an unpaired electron resulting in a local magnetic moment of ∼1 μ_B.

The differential charge densities (Figure 5a,b) illustrate that the transferred charge from K to W_{vac} is primarily located on the three nearest Se atoms, *i.e.*, Se_{1u}, Se_{2u}, and Se_{3u}, while a minor portion of the charge is observable around the next-

DOI: 10.1021/acsnano.8b07595
ACS Nano 2019, 13, 1595−1602

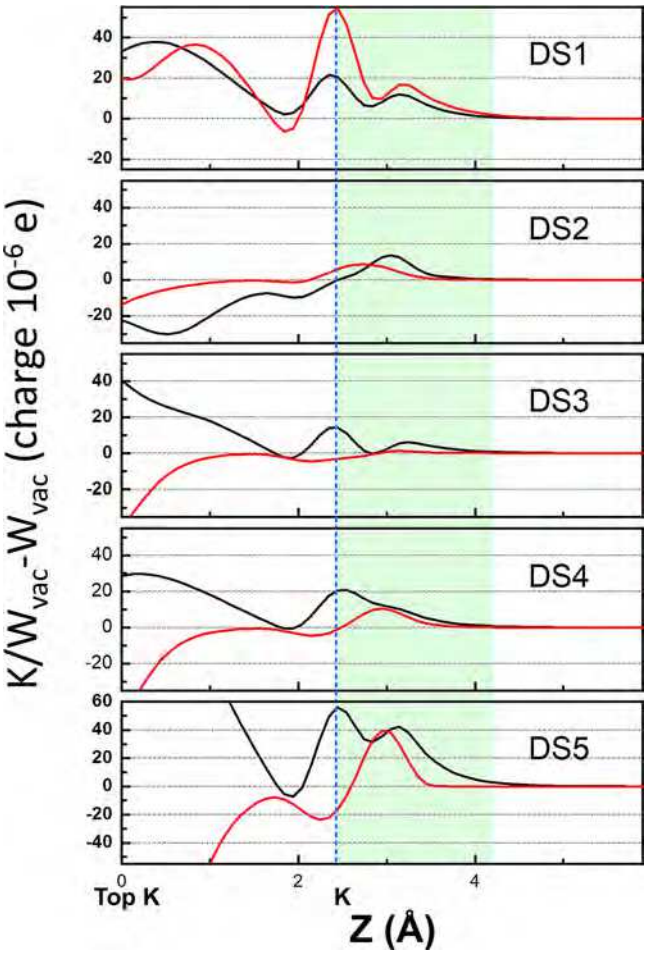

Figure 4. Differences in the spatial distributions of the defect wave functions between the K/W$_{vac}$ and intrinsic W$_{vac}$ as a function of vertical positions (Z). The charge numbers are integrated in a circular cross-section (with a radius of 0.5 Å and centered on the W or the K atom) as ($|\Psi_{K/Wvac}|^2 - |\Psi_{Wvac}|^2$) × S_{cs}. The top Se layer was set to position zero, and the position of the K atom is marked by a blue dashed line. The two spin components for each defect state are plotted in black and red, respectively. For all defect states, the wave functions extend further after the adsorption of a K atom (the shadow region).

nearest Se atoms. Upon K decoration, appreciable charge transfers were observed from the e_g to t_{2g} orbitals of the W atoms around the vacancy, which contribute to the spin density as observed in Figure 5c. The comparable differential charge accumulation (Figure 5b) and spin density (Figure 5c) confirm that the local magnetic moment mainly arises from the charge donated by the K atom and suggest a tunability of spin-exchange coupling by charge doping.[38] Note that the net spin density of the K/W$_{vac}$ point defect spans several unit cells, consistent with a previous study of H atom on graphene.[39]

The existence of the magnetic moment strictly relies on the electron-filling number of these defect levels, namely, whether there is an unpaired spin. As shown in Figure 3d, the Δ_{SS} of the defect states nearly vanishes with one additional electron added to the Se$_{1u}$−Se$_{3u}$ atoms (refer to K/W$_{vac}$+ 1e). In this case, all DS1, DS2, and DS3 are occupied, and all spins are paired. In turn, the splits are restored when there are two extra electrons doped (see K/W$_{vac}$ + 2e in Table S4). Similar behaviors also occur when one and two electrons are removed from the K/W$_{vac}$ complex. In Figure 5d, we show the on/off oscillations of the magnetic moment and the Δ_{SS} as functions of the electron doping level. This finding suggests a promising approach to manipulating the magnetism in ML-WSe$_2$ by tuning the Fermi level *via* a back gate, when the WSe$_2$ flake is placed on an insulating substrate like SiO$_2$ or sapphire.

In the current experiment, the WSe$_2$ sample was grown on a graphite substrate which pins the Fermi level above all defect levels, as evidenced by the almost unchanged locations of conduction band minimum (black dashed line in Figure 2a). As a result, all defect levels are fully occupied without any unpaired spin. Since it is challenging to compute the system with five additional electrons, we thus compare the experimental result with the theoretical calculation of K/W$_{vac}$+1e where the spins are also fully paired. However, with more electrons doped, the defect states level may shift more or less, while the energy separation among them stay nearly unchanged (see Figure S9 for detailed discussions). Therefore, it would be more reasonable to compare the energy separations among P_A−P_D with those in calculations (Figure 3d). In Table 1, we show an excellent agreement between the experiment and calculations for the spin-pairing state. Note that the DS1 of the K/W$_{vac}$/HOPG sample, which should lie below the valence band maximum at the Γ point and is strongly mixed with the valence band states, was not explicitly identified in our STS measurement. The measurements for decay constants, shown in Figure S10, further support the above assignments.

CONCLUSIONS

In conclusion, by the decoration of a single potassium atom, we demonstrated an effective engineering of the W vacancy in ML-WSe$_2$. Combining scanning tunneling microscopy and *ab initio* calculations, we unveiled the appealing modifications on the localized electronic structure. Four defect states, which are invisible in the intrinsic W$_{vac}$, were observed in STS measurement, and their energy levels were quantitatively determined. Calculations revealed an interesting on/off behavior of the magnetic moment and spin splitting at the odd/even number of electron filling in the defect states. In the experiment, the graphite substrate pinned the Fermi level to even filling with spin fully paired, corresponding to an off state, where the calculation and STS measurement have excellent agreement on the defect levels. We expect that our work will create possibilities for spin-based device applications of two-dimensional TMDs, with the advantages of programmable magnetic moment and easy implementation.

METHODS

Monolayer WSe$_2$ was prepared on a HOPG substrate by CVD (see ref 40 for details). Before the STM investigation, the ML WSe$_2$ were cleaned in a UHV chamber (base pressure <1 × 10^{-10} Torr) by heating them up to 200 °C for about 1 h. The potassium was evaporated from a SAES Getters alkali metal dispenser (1.0A, lasting for 5 min) in a UHV chamber (1 × 10^{-10} Torr), while the sample was kept at room temperature. The STM investigations were performed at 77 K in a home-built UHV STM with electrochemically etched W-tips. The dI/dV spectra were taken by using a lock-in amplifier with a modulation voltage of 10 mV at a frequency of 924 Hz. The feedback loop was turned on when taking $(\partial Z/\partial V)_I$ measurements. Therefore, the tip-to-sample distance Z changes correspond to the scanning bias V. By taking a numerical differentiation of Z−V, one obtains the $(\partial Z/\partial V)_I$ spectroscopy.

Density functional theory calculations were performed using the generalized gradient approximation for the exchange-correlation potential, the projector-augmented wave method, and a plane-wave

DOI: 10.1021/acsnano.8b07595
ACS Nano 2019, 13, 1595−1602

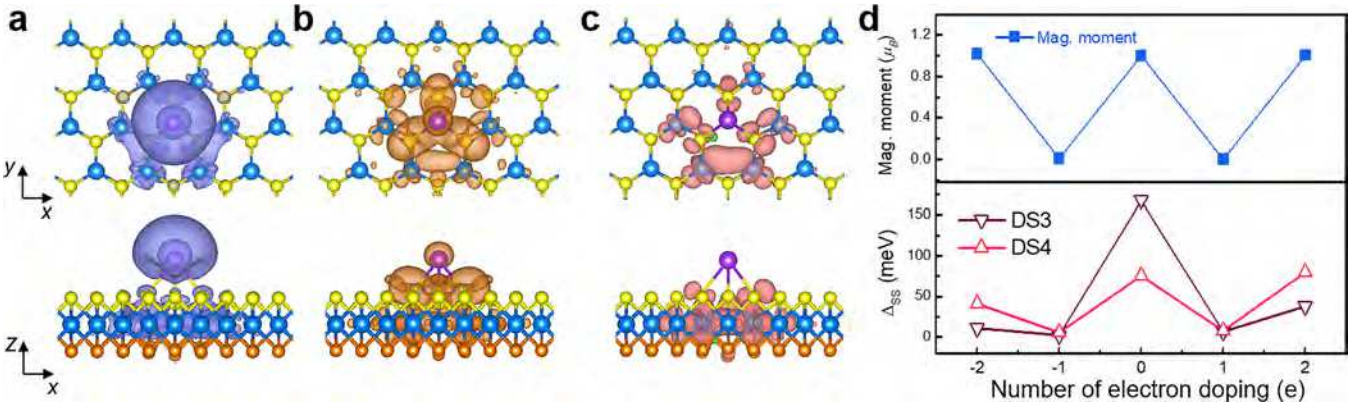

Figure 5. Distributions of the differential charge density/spin density in K/W_{vac} and the dependences of magnetic moment and spin spitting on electron doping level. (a and b) Distributions of differential charge density in K/W_{vac}. The blue and orange isosurfaces in (a) and (b) represent the charge depletion and charge accumulation, respectively. (c) Spin-charge density map of K/W_{vac}. The red and green isosurfaces correspond to charge with different spin orientations. In (a–c), the top and side views are displayed in the upper and lower panels, respectively. (d) Magnetic moment (upper panel) and the spin splitting (lower panel) for DS3 and DS4 as functions of the number of electrons added into a K/W_{vac} complex.

Table 1. Energy Separations of the Defect States in Both the STS Measurements and the Calculation for K/W_{vac}

STS (eV)		K/W_{vac} + 1e (eV)	
$P_A - P_B$	0.340	DS2–DS3	0.345
$P_B - P_C$	**0.210**	DS3–DS4	**0.198**
$P_C - P_D$	**0.110**	DS4–DS5	**0.079**

basis set as implemented in the Vienna ab initio simulation package (VASP). Van der Waals interactions were considered at the vdW-DF level[41,42] with the optB86b[43] functional for the exchange potential (optB86b-vdW), which was proved to be accurate in describing structural related properties of layered materials.[44,45] A 7 × 7 parallelogram supercell was adopted to model the adsorption of a single K atom on WSe_2. The kinetic energy cutoff was set to 400 eV. A 3 × 3 × 1 *k*-mesh was used for all calculations. All atoms were allowed to relax until the residual force on each atom was less than 0.01 eV/Å. The differential charge density shown in Figure 5a,b was derived by $\Delta\rho_d = \rho_0 - \rho_K - \rho_{W_{vac}}$, where ρ_0 is the charge density of K/W_{vac} and $\rho_K$and $\rho_{W_{vac}}$ are those of the K atom and W_{vac} without K adsorption, respectively. The spin density in Figure 5c is derived by subtracting the charge densities of the two spin components. Charge doping on Se or K atoms was realized with the ionic potential method, which was used to model the charge transfer from graphite substrates.[46] The electron doping is evenly applied to the three Se atoms bonding with K atom, *e.g.*, adding $^1/_3$e of each Se in K/W_{vac} + 1e. For hole doping (*i.e.*, -e), the electron was first removed from the K atom by adding a negative potential into the 2*s* core level of K. An additional electron was removed from the valence band by adding a negative potential into the 3p core level of those three Se atoms ($^1/_3$e of each Se) in K/W_{vac} − 2e. This method ensures the doped charges being localized around the Se or K atom and maintains the neutrality of the sample.

ASSOCIATED CONTENT

Supporting Information

The Supporting Information is available free of charge on the ACS Publications website at DOI: 10.1021/acsnano.8b07595.

Additional STM/S data, detailed theoretical discussion of the K adsorption, and summary of Δ_{SS} and magnetic moment for different electron doping levels (PDF)

AUTHOR INFORMATION

Corresponding Authors

*E-mail: cdzhang@whu.edu.cn.
*E-mail: wji@ruc.edu.cn.
*E-mail: shih@physics.utexas.edu.

ORCID

Chendong Zhang: 0000-0002-4960-7036
Wei Ji: 0000-0001-5249-6624
Chih-Kang Shih: 0000-0003-2734-7023

Author Contributions

#C.Z. and C.W. contributed equally.

Notes

The authors declare no competing financial interest.

ACKNOWLEDGMENTS

This work was supported by the National Key R&D Program of China (Grant No. 2018FYA0305800), the National Natural Science Foundation of China (Grant Nos. 11774268, 11622437, and 61674171), the US National Science Foundation (DMR-1306878, DMR-1720595, DMR-1808751, and EFMA-1542747), the Welch Foundation (F-1672), the KAUST (Saudi Arabia), the Academia Sinica (Taiwan) and AOARD-134137 (USA), the Croucher Foundation (Croucher Innovation Award), the RGC of HKSAR (C7036-17W), the Strategic Priority Research Program of Chinese Academy of Sciences (Grant No. XDB30000000), the Fundamental Research Funds for the Central Universities of China, and the Research Funds of Renmin University of China (Grant No. 16XNLQ01). C.W. was supported by the Outstanding Innovative Talents Cultivation Funded Programs 2017 of Renmin University of China. Calculations were performed at the Physics Lab of High-Performance Computing of Renmin University of China and the Shanghai Supercomputer Center.

REFERENCES

(1) Mak, K. F.; Lee, C.; Hone, J.; Shan, J.; Heinz, T. F. Atomically Thin MoS_2: A New Direct-Gap Semiconductor. *Phys. Rev. Lett.* **2010**, *105*, 136805.
(2) Radisavljevic, B.; Radenovic, A.; Brivio, J.; Giacometti, V.; Kis, A. Single-layer MoS2 transistors. *Nat. Nanotechnol.* **2011**, *6*, 147–150.

DOI: 10.1021/acsnano.8b07595
ACS Nano 2019, 13, 1595–1602

(3) Chernikov, A.; Berkelbach, T. C.; Hill, H. M.; Rigosi, A.; Li, Y.; Aslan, O. B.; Reichman, D. R.; Hybertsen, M. S.; Heinz, T. F. Exciton Binding Energy and Nonhydrogenic Rydberg Series in Monolayer WS_2. *Phys. Rev. Lett.* **2014**, *113*, 076802.
(4) Alidoust, N.; Bian, G.; Xu, S. Y.; Sankar, R.; Neupane, M.; Liu, C.; Belopolski, I.; Qu, D. X.; Denlinger, J. D.; Chou, F. C.; Hasan, M. Z. Observation of Monolayer Valence Band Spin-orbit Effect and Induced Quantum Well States in MoX_2. *Nat. Commun.* **2014**, *5*, 4673.
(5) Jones, A. M.; Yu, H.; Ghimire, N. J.; Wu, S.; Aivazian, G.; Ross, J. S.; Zhao, B.; Yan, J.; Mandrus, D. G.; Xiao, D.; Yao, W.; Xu, X. Optical Generation of Excitonic Valley Coherence in Monolayer WSe_2. *Nat. Nanotechnol.* **2013**, *8*, 634−638.
(6) Huang, Y. L.; Ding, Z.; Zhang, W.; Chang, Y.-H.; Shi, Y.; Li, L.-J.; Song, Z.; Zheng, Y. J.; Chi, D.; Quek, S. Y.; Wee, A. T. S. Gap States at Low-Angle Grain Boundaries in Monolayer Tungsten Diselenide. *Nano Lett.* **2016**, *16*, 3682−3688.
(7) Komsa, H. P.; Kotakoski, J.; Kurasch, S.; Lehtinen, O.; Kaiser, U.; Krasheninnikov, A. V. Two-Dimensional Transition Metal Dichalcogenides under Electron Irradiation: Defect Production and Doping. *Phys. Rev. Lett.* **2012**, *109*, 035503.
(8) Rasool, H. I.; Ophus, C.; Zettl, A. Atomic Defects in Two Dimensional Materials. *Adv. Mater.* **2015**, *27*, 5771−5777.
(9) Chen, Y.; Huang, S.; Ji, X.; Adepalli, K.; Yin, K.; Ling, X.; Wang, X.; Xue, J.; Dresselhaus, M.; Kong, J.; Yildiz, B. Tuning Electronic Structure of Single Layer MoS_2 through Defect and Interface Engineering. *ACS Nano* **2018**, *12*, 2569−2579.
(10) Han, Y.; Wu, Z. F.; Xu, S. G.; Chen, X. L.; Wang, L.; Wang, Y.; Xiong, W.; Han, T. Y.; Ye, W. G.; Lin, J. X. Z.; Cai, Y.; Ho, K. M.; He, Y. H.; Su, D. S.; Wang, N. Probing Defect-Induced Midgap States in MoS_2 Through Graphene-MoS_2 Heterostructures. *Adv. Mater. Interfaces* **2015**, *2*, 1500064.
(11) Li, W.-F.; Fang, C.; van Huis, M. A. Strong Spin-orbit Splitting and Magnetism of Point Defect States in Monolayer WS_2. *Phys. Rev. B: Condens. Matter Mater. Phys.* **2016**, *94*, 195425.
(12) Qiu, H.; Xu, T.; Wang, Z. L.; Ren, W.; Nan, H. Y.; Ni, Z. H.; Chen, Q.; Yuan, S. J.; Miao, F.; Song, F. Q.; Long, G.; Shi, Y.; Sun, L. T.; Wang, J. L.; Wang, X. R. Hopping Transport Through Defect-induced Localized States in Molybdenum Disulphide. *Nat. Commun.* **2013**, *4*, 2642.
(13) Lu, C. P.; Li, G. H.; Mao, J. H.; Wang, L. M.; Andrei, E. Y. Bandgap, Mid-Gap States, and Gating Effects in MoS_2. *Nano Lett.* **2014**, *14*, 4628−4633.
(14) Zhu, W. J.; Low, T.; Lee, Y. H.; Wang, H.; Farmer, D. B.; Kong, J.; Xia, F. N.; Avouris, P. Electronic Transport and Device Prospects of Monolayer Molybdenum Disulphide Grown by Chemical Vapour Deposition. *Nat. Commun.* **2014**, *5*, 3087.
(15) He, Y.-M.; Clark, G.; Schaibley, R.; He, Y.; Chen, C.; Wei, Y.-J.; Ding, X.; Zhang, Q.; Yao, W.; Xu, X.; Lu, C.-Y.; Pan, J.-W. Single Quantum Emitters in Monolayer Semiconductors. *Nat. Nanotechnol.* **2015**, *10*, 497−502.
(16) Koperski, M.; Nogajewski, K.; Arora, A.; Cherkez, V.; Mallet, P.; Veuillen, J. Y.; Marcus, J.; Kossacki, P.; Potemski, M. Single Photon Emitters in Exfoliated WSe_2 structures. *Nat. Nanotechnol.* **2015**, *10*, 503−506.
(17) Srivastava, A.; Sidler, M.; Allain, A. V.; Lembke, D. S.; Kis, A.; Imamoğlu, A. Optically Active Quantum Dots in Monolayer WSe_2. *Nat. Nanotechnol.* **2015**, *10*, 491−496.
(18) Hong, J.; Hu, Z.; Probert, M.; Li, K.; Lv, D.; Yang, X.; Gu, L.; Mao, N.; Feng, Q.; Xie, L.; Zhang, J.; Wu, D.; Zhang, Z.; Jin, C.; Ji, W.; Zhang, X.; Yuan, J.; Zhang, Z. Exploring Atomic Defects in Molybdenum Disulphide Monolayers. *Nat. Commun.* **2015**, *6*, 6293.
(19) Zhou, W.; Zou, X. L.; Najmaei, S.; Liu, Z.; Shi, Y. M.; Kong, J.; Lou, J.; Ajayan, P. M.; Yakobson, B. I.; Idrobo, J. C. Intrinsic Structural Defects in Monolayer Molybdenum Disulfide. *Nano Lett.* **2013**, *13*, 2615−2622.
(20) Lin, Y. C.; Bjorkman, T.; Komsa, H. P.; Teng, P. Y.; Yeh, C. H.; Huang, F. S.; Lin, K. H.; Jadczak, J.; Huang, Y. S.; Chiu, P. W.; Krasheninnikov, A. V.; Suenaga, K. Three-fold Rotational Defects in Two-dimensional Transition Metal Dichalcogenides. *Nat. Commun.* **2015**, *6*, 6736.
(21) Erementchouk, M.; Khan, M. A.; Leuenberger, M. N. Optical Signatures of States Bound to Vacancy Defects in Monolayer MoS_2. *Phys. Rev. B: Condens. Matter Mater. Phys.* **2015**, *92*, 121401.
(22) Noh, J. Y.; Kim, H.; Kim, Y. S. Stability and Electronic Structures of Native Defects in Single-layer MoS_2. *Phys. Rev. B: Condens. Matter Mater. Phys.* **2014**, *89*, 205417.
(23) González, C.; Biel, B.; Dappe, Y. J. Theoretical Characterisation of Point Defects on a MoS_2 Monolayer by Scanning Tunnelling Microscopy. *Nanotechnology* **2016**, *27*, 105702.
(24) Park, J. H.; Sanne, A.; Guo, Y. Z.; Amani, M.; Zhang, K. H.; Movva, H. C. P.; Robinson, J. A.; Javey, A.; Robertson, J.; Banerjee, S. K.; Kummel, A. C. Defect Passivation of Transition Metal Dichalcogenides *via* a Charge Transfer van der Waals Interface. *Sci. Adv.* **2017**, *3*, No. e1701661.
(25) Vancsó, P.; Magda, G. Z.; Peto, J.; Noh, J. Y.; Kim, Y. S.; Hwang, C.; Biro, L. P.; Tapaszto, L. The Intrinsic Defect Structure of Exfoliated MoS_2 Single Layers Revealed by Scanning Tunneling Microscopy. *Sci. Rep.* **2016**, *6*, 29726.
(26) Zhang, S.; Wang, C.-G.; Li, M.-Y.; Huang, D.; Li, L.-J.; Ji, W.; Wu, S. Defect Structure of Localized Excitons in a WSe_2 Monolayer. *Phys. Rev. Lett.* **2017**, *119*, 046101.
(27) Fuhr, J. D.; Saul, A.; Sofo, J. O. Scanning Tunneling Microscopy Chemical Signature of Point Defects on the MoS_2(0001) Surface. *Phys. Rev. Lett.* **2004**, *92*, 026802.
(28) Kobayashi, K.; Yamauchi, J. Electronic Structure and Scanning Tunneling Microscopy Image of Molybdenum Dichalcogenide Surfaces. *Phys. Rev. B: Condens. Matter Mater. Phys.* **1995**, *51*, 17085−17095.
(29) Altibelli, A.; Joachim, C.; Sautet, P. Interpretation of STM images: the MoS_2 surface. *Surf. Sci.* **1996**, *367*, 209−220.
(30) Perrot, E.; Humbert, A.; Piednoir, A.; Chapon, C.; Henry, C. R. STM and TEM Studies of a Model Catalyst: Pd/MoS_2(0001). *Surf. Sci.* **2000**, *445*, 407−419.
(31) Ugeda, M. M.; Bradley, A. J.; Shi, S.-F.; da Jornada, F. H.; Zhang, Y.; Qiu, D. Y.; Ruan, W.; Mo, S.-K.; Hussain, Z.; Shen, Z.-X.; Wang, F.; Louie, S. G.; Crommie, M. F. Giant Bandgap Renormalization and Excitonic Effects in a Monolayer Transition Metal Dichalcogenide Semiconductor. *Nat. Mater.* **2014**, *13*, 1091−1095.
(32) Zheng, Y.; Chen, Y.; Huang, Y.; Gogoi, P. K.; Li, M.-Y.; Li, L.-J.; Trevisanutto, P. E.; Wang, Q.; Pennycook, S. J.; Wee, A. T. S.; Quek, S. Y. . *Origin of Single Photon Emission in 2D WSe_2*, **2018**.
(33) Barja, S.; Refaely-Abramson, S.; Schuler, B.; Qiu, D. Y.; Pulkin, A.; Wickenburg, S.; Ryu, H.; Ugeda, M. M.; Kastl, C.; Chen, C.; Hwang, C.-Y.; Schwartzberg, A.; Aloni, S.; Mo, S.-K.; Ogletree, D.-F.; Crommie, M. F.; Yazyev, O. V.; Louie, S. G.; Neaton, J. B.; Weber-Bargioni, A. . *Identifying Substitutional Oxygen as a Prolific Point Defect in Monolayer Transition Metal Dichalcogenides with Experiment and Theory*, **2018**.
(34) Zhang, Y.; Chang, T. R.; Zhou, B.; Cui, Y. T.; Yan, H.; Liu, Z. K.; Schmitt, F.; Lee, J.; Moore, R.; Chen, Y. L.; Lin, H.; Jeng, H. T.; Mo, S. K.; Hussain, Z.; Bansil, A.; Shen, Z. X. Direct Observation of the Transition from Indirect to Direct Bandgap in Atomically Thin Epitaxial $MoSe_2$. *Nat. Nanotechnol.* **2013**, *9*, 111−115.
(35) Zhu, F.-f.; Chen, W.-j.; Xu, Y.; Gao, C.-l.; Guan, D.-d.; Liu, C.-h.; Qian, D.; Zhang, S.-C.; Jia, J.-f. Epitaxial Growth of Two-dimensional Stanene. *Nat. Mater.* **2015**, *14*, 1020−1025.
(36) Zhang, P.; Richard, P.; Xu, N.; Xu, Y.-M.; Ma, J.; Qian, T.; Fedorov, A. V.; Denlinger, J. D.; Gu, G. D.; Ding, H. Observation of an Electron Band above the Fermi Level in $FeTe_{0.55}Se_{0.45}$ from *in-situ* Surface Doping. *Appl. Phys. Lett.* **2014**, *105*, 172601.
(37) Zhang, C.; Chen, Y.; Johnson, A.; Li, M.-Y.; Li, L.-J.; Mende, P. C.; Feenstra, R. M.; Shih, C.-K. Probing Critical Point Energies of Transition Metal Dichalcogenides: Surprising Indirect Gap of Single Layer WSe_2. *Nano Lett.* **2015**, *15*, 6494−6500.
(38) Wang, C.; Zhou, X.; Pan, Y.; Qiao, J.; Kong, X.; Kaun, C.-C.; Ji, W. Layer and Doping Tunable Ferromagnetic Order in Two-

DOI: 10.1021/acsnano.8b07595
ACS Nano 2019, 13, 1595−1602

dimensional CrS_2 layers. *Phys. Rev. B: Condens. Matter Mater. Phys.* **2018**, *97*, 245409.
(39) Gonzalez-Herrero, H.; Gomez-Rodriguez, J. M.; Mallet, P.; Moaied, M.; Palacios, J. J.; Salgado, C.; Ugeda, M. M.; Veuillen, J. Y.; Yndurain, F.; Brihuega, I. Atomic-scale Control of Graphene Magnetism by Using Hydrogen Atoms. *Science* **2016**, *352*, 437−441.
(40) Huang, J. K.; Pu, J.; Hsu, C. L.; Chiu, M. H.; Juang, Z. Y.; Chang, Y. H.; Chang, W. H.; Iwasa, Y.; Takenobu, T.; Li, L. J. Large-Area Synthesis of Highly Crystalline WSe_2 Mono Layers and Device Applications. *ACS Nano* **2014**, *8*, 923−930.
(41) Lee, K.; Murray, É. D.; Kong, L.; Lundqvist, B. I.; Langreth, D. C. Higher-accuracy van der Waals Density Functional. *Phys. Rev. B: Condens. Matter Mater. Phys.* **2010**, *82*, 081101.
(42) Dion, M.; Rydberg, H.; Schröder, E.; Langreth, D. C.; Lundqvist, B. I. Van der Waals Density Functional for General Geometries. *Phys. Rev. Lett.* **2004**, *92*, 246401.
(43) Klimeš, J.; Bowler, D. R.; Michaelides, A. Van der Waals Density Functionals Applied to Solids. *Phys. Rev. B: Condens. Matter Mater. Phys.* **2011**, *83*, 195131.
(44) Hu, Z.-X.; Kong, X.; Qiao, J.; Normand, B.; Ji, W. Interlayer Electronic Hybridization Leads to Exceptional Thickness-dependent Vibrational Properties in Few-layer Black Phosphorus. *Nanoscale* **2016**, *8*, 2740−2750.
(45) Qiao, J.; Pan, Y.; Yang, F.; Wang, C.; Chai, Y.; Ji, W. Few-layer Tellurium: One-dimensional-like Layered Elementary Semiconductor with Striking Physical Properties. *Science Bulletin* **2018**, *63*, 159−168.
(46) Ji, W.; Lu, Z.-Y.; Gao, H. Electron Core-Hole Interaction and Its Induced Ionic Structural Relaxation in Molecular Systems under X-Ray Irradiation. *Phys. Rev. Lett.* **2006**, *97*, 246101.

DOI: 10.1021/acsnano.8b07595
ACS Nano 2019, 13, 1595−1602